

Shear demands of rock-socketed piles subject to cyclic lateral loading

Rabie Farrag¹, Carter Cox², Benjamin Turner³, and Anne Lemnitzer⁴*

Abstract: The determination of internal pile reactions is critical to designing and assessing the structural performance of deep foundations. Internal shear and moment profiles strongly depend on lateral pile-soil interaction, which in turn depends on pile and soil stiffnesses as well as the stiffness contrast between soft and stiff strata, such as occurs at a soil/rock interface. At zones of strong geomaterial stiffness contrast, Winkler-spring-type analyses predict abrupt changes in the internal pile reactions for laterally-loaded foundation elements. In particular, the sudden deamplification of internal moments when transitioning from a soft to stiff layer is accompanied by amplification of pile shear. This "shear spike" can result in bulky transverse reinforcement designs for drilled shaft rock sockets that pose constructability challenges due to reinforcement congestion, increasing the risk of defective concrete on the outside of the cage. This paper presents an experimental research program of three large-scale, instrumented drilled shafts with simulated rock sockets constructed from concrete. Each shaft had a different transverse reinforcement design intended to bound the amplitude of the predicted amplified shear demand, with a particular emphasis on performance of shafts with shear resistance less than the predicted demand and below the code minimum. Test results suggested that the shafts experienced a flexure-dominated failure irrespective of the transverse reinforcement detailing.

Keywords: piles, lateral loading, stiffness contrast, rock sockets, shear reinforcement

Introduction

Deep foundation systems are an integral albeit costly component of our urban living and infrastructure system. In areas where soft soils dominate subsurface conditions, piles are extensively used to transfer vertical and lateral superstructure loading originating from tall buildings, bridges, or offshore structures into stronger ground. Tip embedment into a strong geomaterial layer, such as a drilled shaft rock socket, offers an attractive solution for achieving maximum tip resistance and improving the load transfer behavior of the foundation element. Previous experimental research on laterally loaded rock-socketed piles predominantly focused on the geotechnical aspects of rock-socketed piles and the derivation of p-y relationships

for rock materials (e.g., Frantzen and Stratten, 1987; Carter and Kulhawy, 1992; Dykeman and Valsangkar, 1996; Gabr et al., 2002: Parsons et al., 2010: Guo and Lehane, 2016).

Stiffness contrasts between rock and softer surface soils have historically challenged design engineers attempting to capture the pile structural response in the vicinity of the stiffness interface. Particularly, predictions using Winkler-springtype analyses yield abrupt changes in the pile moment profile which translates into amplified shear force at the interface boundary of stiff and soft geomaterial layers. This amplification is a byproduct of the one-dimensional nature of the beam-column representation that is solved through differentiation of the governing fourth-order differential equation relating geomaterial reactions to internal pile reactions. The foundation engineering community has experienced much controversy over whether the large resulting shear demands are representative of actual force effects that must be designed for, or if amplified shear forces are artifacts of the Winklerspring-type analysis methodology that can be ignored or addresses with a "workaround" solution. Nationally recognized manuals such as the Caltrans "Bridge Design Practice Manual" (Section 16.4.4.4) acknowledge this controversy: "When CIDH piles [cast-in-drilled-hole, i.e., drilled shafts] tipped in rock are analyzed for lateral loads, the p-y method reports shear demand forces that exceed the seismic overstrength shear, V_o calculated demand in the column. The abrupt change to high-stiffness p-y springs may amplify shear force to more than 5V within the rock socket. ... However, there is an

© 2020. The Author(s). Published by The Deep Foundations Institute. Print ISSN: 1937-5247 Online ISSN: 1937-5255 This is an Open Access article distributed under the terms of the Creative Commons Attribution License (https://creativecommons.org/licenses/by/4.0/), which permits unrestricted copies and distribution in any medium or format, and adaptation provided the original work is properly cited. Received 26 May 2020; received in revised form 10 September 2020; accepted 29 September 2020 https://doi.org/10.37308/DFIJnl.20200526.223

PhD Student Researcher, Dept of Civil & Environmental Engineering, 4135 Engineering Gateway, University of California, Irvine, Īrvine, CA, 92697, USA

Structural Engineer, HDR Inc., 3230 El Camino Real #200, Irvine, CA, 92617, USA

Senior Engineer, Dan Brown and Associates, 1440 Las Encinas Drive, Los Osos, CA, 93402, USA

Associate Professor, Dept of Civil & Environmental Engineering, 4135 Engineering Gateway, University of California, Irvine, Irvine,

Corresponding author, email: alemnitz@uci.edu

ongoing debate over whether the design force is "real" and whether the discretization of distributed soil reaction to nodal springs is appropriate at the rock interface." (Caltrans, 2015).

On many projects, the structural designer will proportion the transverse reinforcement to satisfy the amplified shear demand, often without adequate consideration of the constructability concerns that this may cause. In a prescriptive design setting, an unintended consequence of this approach is that the designer may be exposed to liability for resulting defects if the contractor claims that the congested cage design is what led to defective concrete, not their own means and methods. In contrast, some designers attempt to mitigate this issue through various approaches that fall into the category of "engineering judgment"; for example, by artificially redistributing the shear profile over a larger depth interval while maintaining the same total magnitude of shear resistance (i.e., area under the shear curve), effectively disregarding the predicted local shear spike. A related approach is to simulate a gradual increase in stiffness of the rock layer with depth, thereby reducing the magnitude of stiffness contrast at the soil-rock boundary and consequently forcing the moment to distribute over a larger depth interval, resulting in reduced shear amplification. In cases where there is a gradual increase in rock stiffness, for example because of intense weathering at the rock surface that gradually diminishes with depth, this approach is appropriate because it reflects the real ground conditions. But to artificially simulate the rock in this manner if such a transition is not supported by rock core data cannot be scientifically justified. While the authors are not aware of any instances in which these approaches have been associated with a foundation failure, it has not yet been demonstrated that the underlying concepts can be supported by valid, rigorous analyses.

The validation of shear amplification (or the lack thereof) predicted with the p-y method against instrumented load tests or validated numerical models is limited in existing literature. However, the correct evaluation of shear demands at soil-rock interfaces is vital since the shear demand may govern the drilled shaft structural design. High shear demands require high transverse reinforcement ratios, which in turn impacts the overall constructability of the foundation system. One of the most commonly encountered adverse effects of increased demands in transverse reinforcement is the obstruction of concrete flow and the formation of air pockets, as illustrated in Figure 1. Numerical research has attempted to provide insight into the principal mechanism (e.g., Arduino et al., 2018), but no conclusive recommendations are available that can provide sufficient fundamental understanding or data validation to provide informed and reliable alternative design recommendations suitable for routine practice. To date, Arduino et al. is the only study that investigated the effects of shear magnification by numerically assessing the pile behavior at the rock-soil boundary via parametric studies using the FEM software platform OpenSees (McKenna et al., 2000). Other literature documenting lateral behavior of rock-socketed piles primarily focused on the overall lateral load behavior (Rojas-Gonzales et al., 1993, Yang and Liang, 2006; Guo and Lehane, 2016), analytical and numerical studies of

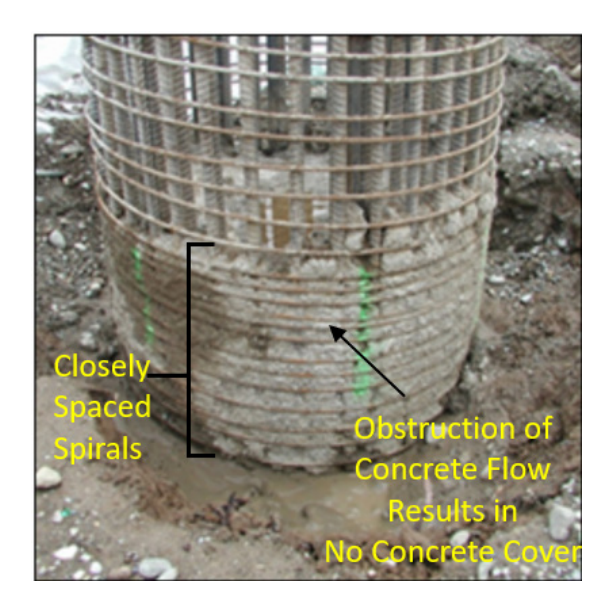


Figure 1. Defective concrete associated with close rebar spacing in piles (after Brown $\it et al., 2010$)

pile performance in various rock-types, embedment lengths, and the investigation of suitable modeling techniques (e.g., Brown and Shie, 1990; Carter and Kulhawy, 1992; Dykeman and Valsangkar, 1996; Leung and Chow, 2000; Ashour and Norris, 2001; Ramakrishna *et al.*, 2004, Yuan *et al.*, 2014), as well as the derivation of soil resistance formulations for piles in rock (i.e., *p-y* curves) (e.g., Frantzen and Stratton, 1987; Reese, 1997; Gabr *et al.*, 2002; Liang *et al.*, 2009; Kim *et al.*, 2015; Koshravifar and Zafir, 2019)

This manuscript presents the first study to investigate the shear behavior of laterally loaded drilled shafts on an experimental basis.

Experimental Program

The experimental studies were executed in the "soil pit" at the Structural Engineering Testing Hall of the University of California, Irvine. Three test piles were embedded in a constructed sand-over-rock stratigraphy and subjected to reverse cyclic lateral loading until complete structural failure was reached. The "rock" was constructed from cast-in-place concrete blocks that were post-tensioned to the base of the test pit to provide translational and rotational restraint meant to simulate a continuous mass of strong rock. The specimen design and configuration were determined partly on the basis of analytical pre-test predictions using the commercially available software platform LPILE (Ensoft, 2018). This method of analysis is herein referred to generically as the "p-v method." The analytical results enabled the iteration of suitable specimen geometries and reinforcement configurations that would serve three objectives: (1) to gain general insight into the piles' nonlinear performance behavior and failure mechanism, (2) to learn whether the amplification of shear forces at the geomaterial stiffness boundary predicted using the p-y method are consistent with measured values, and (3) to assess the behavior and lateral failure mechanism of shafts with transverse reinforcement resistances less than the shear demand predicted using the p-y method.

Geomaterial layer properties and geometry were specified such that the stiffness contrast creates a significant shear amplification relative to the applied lateral load at the pile head as predicted using the p-y method. Initial estimates of the sand properties were based on information provided by the material supplier. Concrete strengths were taken as 28-day design compressive strengths. Within LPILE, the rock layer was analytically represented using p-y springs for weak rock (Reese 1997) and the sand was modeled using the O'Neill and Murchison (1983) p-y model. The input parameters for the simulated rock layer consisted of initial rock mass modulus, uniaxial compressive strength, strain factor, and rock quality designation (RQD), taken as 32,888 MPa [4770 ksi], 48 MPa [7 ksi], 0.0005, and 100%, respectively. Model parameters for the sand layer consisted of effective unit weight and friction angle taken as 14.5kN/m³ [92 pcf] and 35 degrees. The planned tests were simulated up to a maximum applied lateral load at the pile head of 58 kN [13 kips], where the lateral load is applied approximately 175 cm [6 ft] above the sand surface to amplify flexural demands and maximize the lateral demands reaching the rock socket. For the final selected stratigraphic configuration, the amplified shear calculated with LPILE is 471 kN [106 kips], which corresponds to a shear amplification ratio of 8.1 (i.e., the applied shear normalized by calculated amplified shear).

The three 18.0-in diameter pile specimens were designed as follows: Specimen 1 was designed to resist maximum values of shear and moment predicted using LPILE, which required significant shear reinforcement - a No. 4 spiral at 114-mm [4.5-in] pitch ($\rho_s = 1.27\%$). Specimen 2 $(\rho = 0.96\%)$ was designed to only satisfy the code minimum volumetric transverse reinforcement requirements (ACI 318, 2019, AASHTO, 2017) associated with the applied lateral load, and did not provide adequate calculated nominal shear strength to resist the predicted amplified shear demand. Specimen 3 only contained a minimal amount of transverse reinforcement ($\rho_s = 0.26\%$), which provided adequate calculated nominal shear resistance to exceed the applied lateral load (58 kN/13 kips) but did not satisfy code minimum requirements for transverse reinforcement spacing and did not provide adequate calculated nominal shear strength to resist the predicted amplified shear demand. If the actual shear amplification at the soil-rock interface is consistent with the value predicted using the p-y method, and the nominal shear strength of the structural sections are reasonably close to the calculated values, Specimens 2 and 3 would be expected to fail due to insufficient shear strength in the upper rock socket region where the predicted shear spike occurs. A structural design summary for all specimens is presented in Table 1.

Figure 2 shows the predicted pile moment and shear profiles for the three pile specimens at the point when the calculated maximum moment reaches the nominal flexural strength of the section. (It is noted that nominal flexural strength is not assumed to depend on the variable transverse reinforcement details of each specimen for this purpose.) Figure 2(b) illustrates shear amplification at the soil-rock boundary. The significant predicted shear amplification ratio

was intentionally created to exaggerate the analyticallypredicted shear spike effect, although this amount of shear amplification is not uncommon in practice for real project geometries and stratigraphy. Furthermore, the research team hypothesized that structural shear failure would not occur despite the significant discrepancy between calculated nominal shear strength and amplified shear demand, and that the shafts would form a flexural mechanism when loaded to failure; the significant shear amplification was intended to test this hypothesis. Likewise, the thickness of the sand layer was minimized and it was placed in a relatively loose condition to maximum lateral demands reaching the socket while still representing the commonly encountered soil-over-rock stratigraphy. The dashed lines in Figure 2 indicate the nominal shear strength (V_n) of each specimen. These shear strengths (also shown in Table 1) are predicted to be reached when the piles experience lateral pile head loads of 13kN, 11.6kN, and 7.8 kN [58kips, 52kips, and 35 kips] for Specimens 1, 2, and 3, respectively (presented as "predicted pile head load at failure" in Table 1).

Specimen Geometry and Reinforcement

The reinforced concrete piles were 4.57 m [15.0 ft] in length and 0.46 m [18.0 in] in diameter. As shown schematically in Figure 3, the piles were embedded in 1.20 m [4.0 ft] of "rock", simulated experimentally by high strength concrete (f' = 48.3MPa [7 ksi]). The concrete blocks (i.e., the "rock sockets") had dimensions of 1.83 m [6.0 ft] in length, 1.22 m [4.0 ft] in width, and 1.22 m [4.0 ft] in height. The blocks were secured to the reinforced concrete floor of the testing facility using pre-drilled, epoxy-grouted, high strength steel anchors. The piles extended a total of 3.35 m [11.0 ft] above the rock. A rectangular "pile cap" with cross-sectional dimensions of 0.61 x 0.61 m [24 x 24 in] and a height of 0.41m [16 in] was constructed at each pile head and used for actuator attachment and application of lateral loading. The reinforcement configurations of the three specimens are illustrated in Figure 3. Longitudinal reinforcement consisted of eight No. 6 Grade 60 A706 steel bars ($A_{s, total} = 22.71 \text{ cm}^2 [3.52 \text{ in}^2]$), which corresponds to a longitudinal reinforcement ratio of $\rho = 1.41\%$.

Longitudinal rebars were equally spaced around the circumference of the pile with a clear concrete cover of 5 cm [2.0 in]. Specimens 1 and 2 transverse reinforcement consisted of #4 spirals, and Specimen 3 transverse reinforcement consisted of #3 ties as indicated in Figure 3. The transverse reinforcement of Specimen 1 (#4 spirals) was spaced at a pitch of 114 mm [4.5 in] in the rock socket (i.e., approximately up to an elevation of 1.2 m [4.0 ft] from the pile tip), and spaced at a pitch of 152 mm [6.0 in] along the remaining pile height. The closer spiral pitch at the bottom of the pile is the only configuration that satisfies the amplified shear demand within the rock socket as predicted by the p-y analysis shown in Table 1 and Figure 2. Specimen 2 was reinforced with #4 transverse spirals at a pitch of 152 mm [6.0 in] along the entire pile length. The transverse reinforcement consisted of #3 ties spaced at 305 mm [12.0 in] across the entire pile length and provided just enough structural stability to

Table 1. Predictions of pile demands using LPILE, selected reinforcement, and calculated resistances

	Specimen 1 (SP1)	Specimen 2 (SP2)	Specimen 3 (SP3)
Designed to satisfy:	Amplified shear	Code minimum	Applied shear
Max applied load @ pile head, kN [kips]	58 [13]		
Max. flexure demands M _u , kN-m [kip-ft]	149 [110]	149 [110]	149 [110]
Nominal moment strength M _n , kN-m [kip-ft]	150 [111]	150 [111]	150 [111]
Maximum shear demand V _u , kN [kips]	471 [106]	471 [106]	471 [106]
Concrete shear strength V _c , kN [kips]	155 [34.8]	155 [34.8]	155 [34.8]
Steel shear strength (required) V _s , kN [kips]	320 [72]	Not needed/Use min.	Not needed
Selected transverse reinforcement, bar # @ pitch, mm [in]	Spiral #4 @ 114 [4.5]	Spiral #4 @ 152 [6]	Ties #3 @ 305[12]
Transverse reinf. volumetric ratio, ρ_s [%]	1.27%	0.95%	0.26%
Nominal shear strength V _n , kN [kips]	477 [107]	396 [89]	222 [50]
Predicted failure mode based on <i>p-y</i> analysis	Flexural failure	Shear failure	Shear failure
Predicted pile head load at failure based on <i>p-y</i> analysis, kN [kip]	58 [13]	52 [11.6]	35 [7.8]

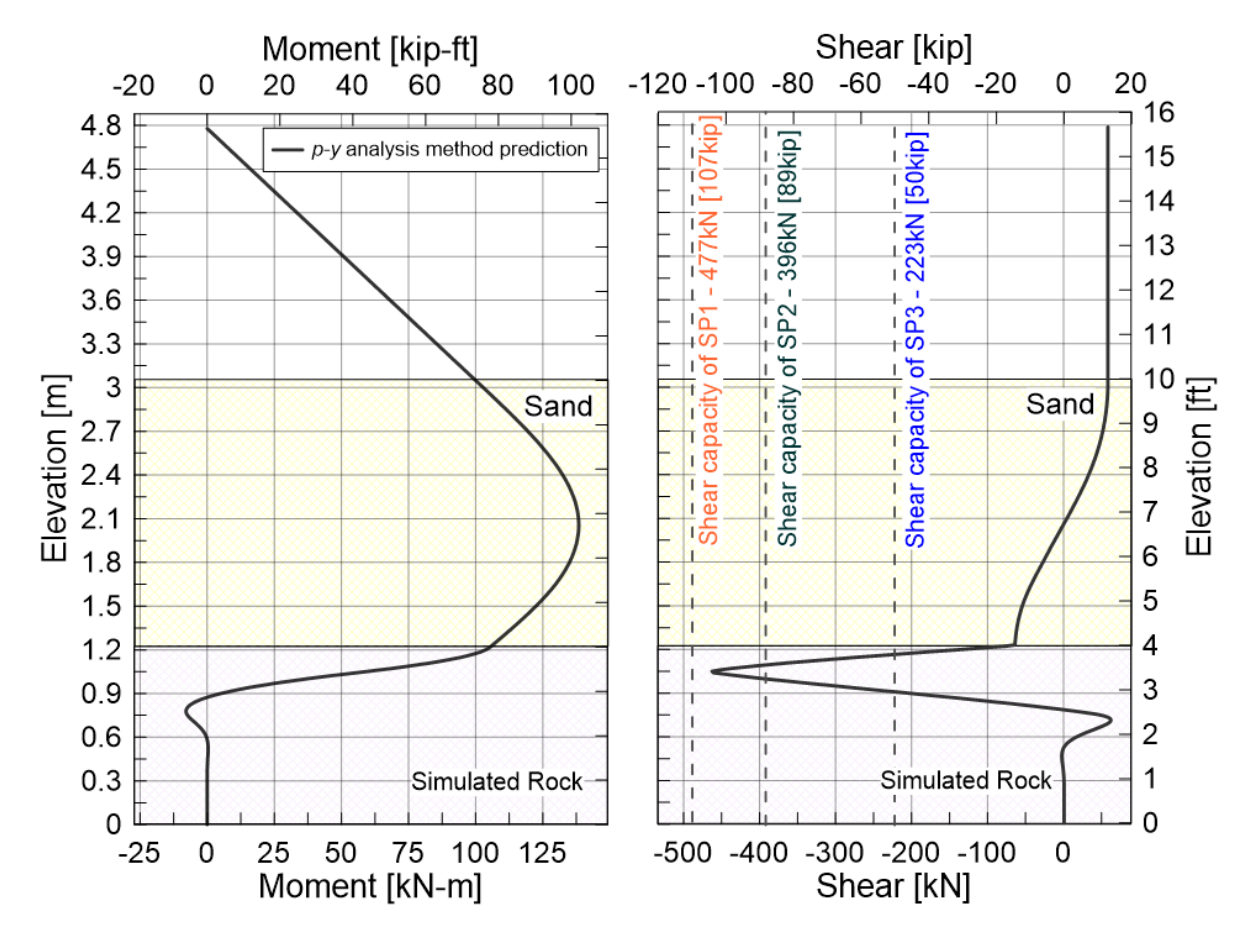


Figure 2. Prediction of pile moment (left) and shear (right) due to a lateral load of 58 kN (13 kips) applied at the pile head

hold the longitudinal rebar cage together. Specimen's 3 transverse reinforcement ratio is only 0.26%. Its contribution to the overall shear strength $V_{\rm n}$ is minimal and analytically not needed, as the concrete cross-section provides adequate shear resistance $V_{\rm c}$ to satisfy the applied lateral load demands at the pile head (i.e., shear amplification at the rock socket is

ignored and the internal shear force is assumed to distribute uniformly as the case for cantilever beams.) This scenario implies that the assumed shear magnitude is equal to the applied lateral force at the pile head. To reiterate, this configuration is not permitted by any structural design codes and was intended for experimental demonstration purposes only.

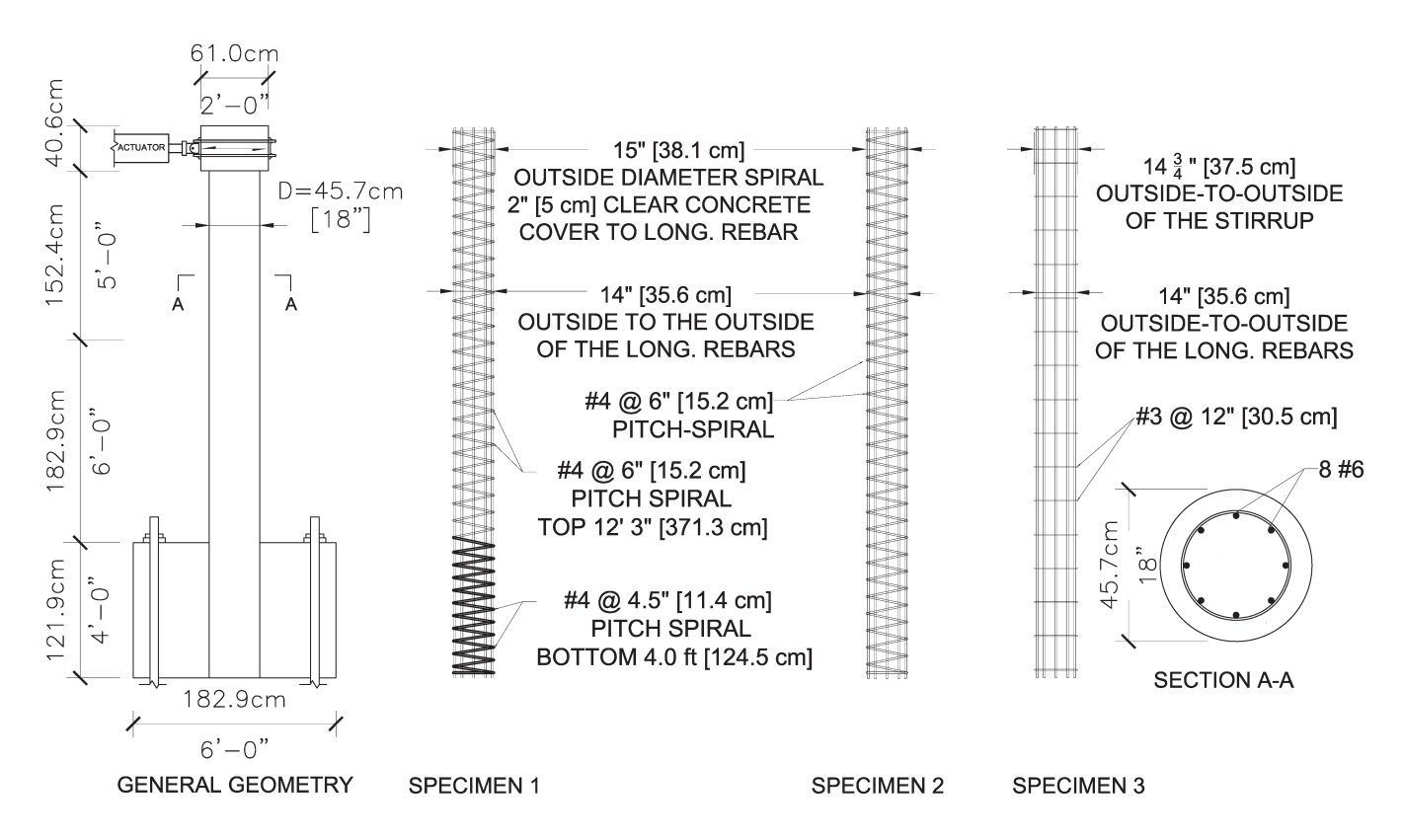


Figure 3. Schematic specimen configuration and variation of transverse reinforcement for all specimens

Specimen Instrumentation

Specimen instrumentation consisted of external and internal sensors including linear voltage differential transducers (LVDT), string potentiometers (SP), inclinometers, and strain gauges in longitudinal (E/W) directions, as well as rosette (R), and tetrahedral configurations (T). Strain gauges arranged in rosette configuration were placed as surface strain gauges on the exterior concrete surface of the pile, and strain gauges attached to a tetrahedral sensor carrier were placed inside the pile section to capture internal shear strains (separate publication to follow). A schematic instrumentation plan for Specimen 1 is shown in Figure 4.

Soil Material

The sand material was selected based on the following criteria: (1) ease of installation and pluviation into the soil pit, (2) local availability, (3) properties being representative of typical loose in-situ granular soil, and (4) costs associated with material and transportation to UCI. Prior to selecting the final soil material, about a dozen fill materials from different suppliers were investigated in the laboratory to identify their mechanical and index properties. The final choice consisted of a fill sand with a friction angle of 34.6 deg and a cohesion of 4.96 kN/m² [0.72 psi] determined through direct shear testing per ASTM D3080, and a maximum dry unit weight of 21 kN/m³ [134 pcf] determined via modified Proctor compaction testing (ASTM D1557). The sand was pluviated from a minimum height of 3.66 m [12 ft] to reach a target average relative density of 20% (Figure 8g).

Pluviation was accomplished using a self-designed and calibrated sieve system attached at the bottom of a concrete hopper. The calibration process included the iteration of optimum freefall heights as well as the assembly of multiple sieve openings until the desired relative density was reached. The low in-situ relative density of 20% provided a strong stiffness contrast between the soil and simulated rock. The average in-situ moisture content of the soil was 6%. Flat Dilatometer testing (DMT/ASTM D6635) was carried out to determine the in-situ characteristics of the sand after pluviation was completed. Following Marchetti (1980), the material index (I_D), horizontal stress index (K_D), and dilatometer modulus (E_D) were evaluated using Equations 1, 2, and 3, where $p_0 = \text{contact pressure need-}$ ed prior to membrane expansion, p₁ = contact pressure to produce a membrane displacement of 1.1mm, $u_0 = pore$ water pressure, σ'_0 = in-situ vertical effective stress, and μ_{s} = soil Poisson's ratio. I_{D} , K_{D} , and E_{D} were determined to be 1.5 MPa [217 psi], 2.8 MPa [406 psi], and 2.08 MPa [301 psi], respectively. The soil's elasticity modulus, E_z, can be obtained from the dilatometer modulus using Equation 4. The soil friction angle can be back-calculated from the horizontal stress index K_D using Equation 5. The variation of soil's elasticity modulus and friction angle versus depth are shown in Figure 5. The average in-situ friction angle was found to be 33° and the average soil modulus (E₂) was approximately 1.89 MPa [274 psi]. Additional in-situ testing of the soil material via Cone Penetration Testing (CPT per ASTM D5778) was used to estimate the soil average

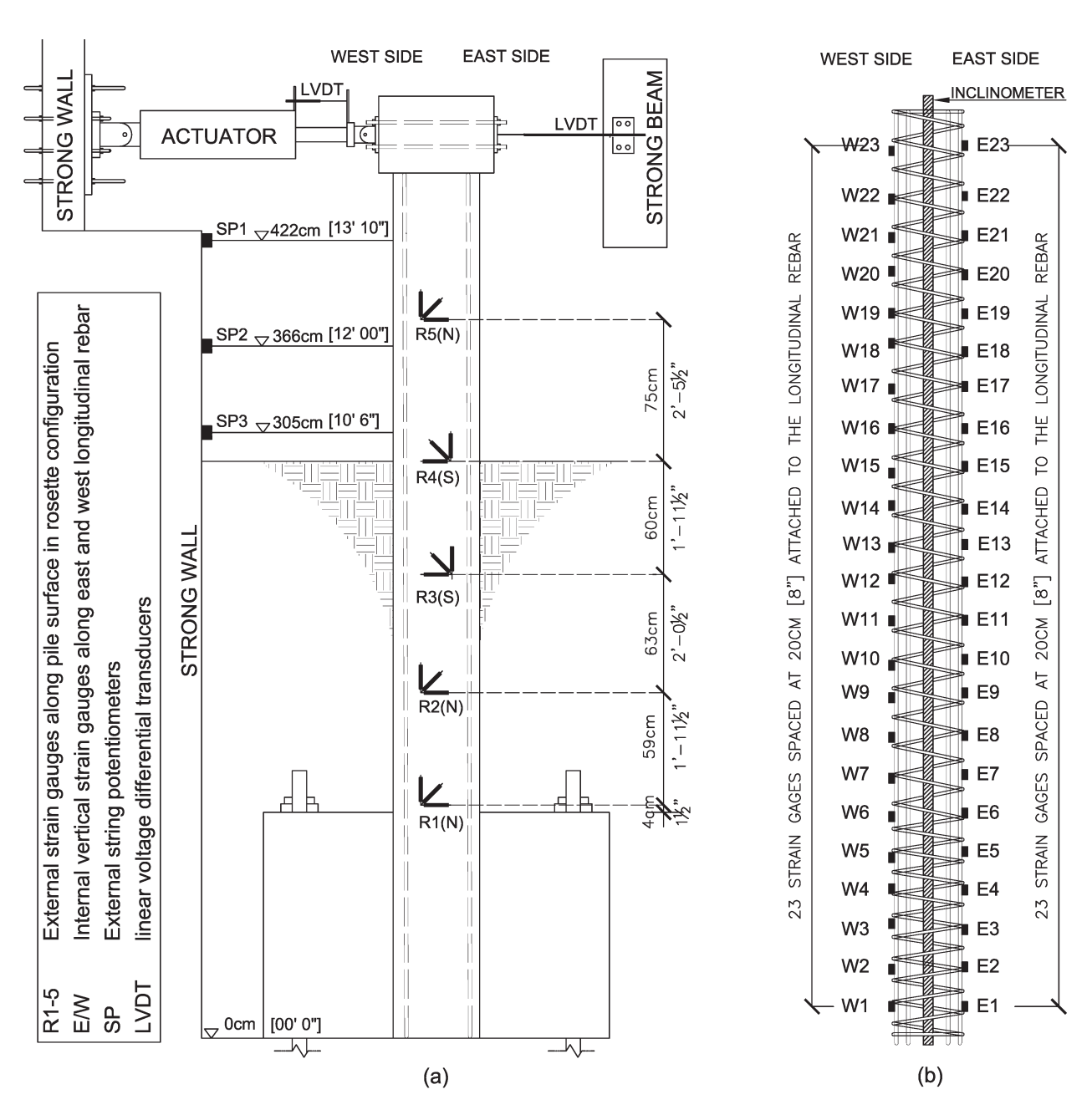


Figure 4. Instrumentation layout for Specimen 1: (a) external sensors; and (b) internal sensors (tetrahedral sensors not shown)

Young's modulus (E_s) of 1.85 MPa [268 psi]. SCPT shear wave velocity measurements suggested an average shear wave velocity (V_s) of 220 m/s [722 ft/s]; a graphical presentation of test results is omitted for brevity.

$$I_D = p_1 - p_2 / p_0 - u_0 \tag{1}$$

$$K_D = p_1 - u_0 / \sigma_0' \tag{2}$$

$$E_D = 34.7(p_1 - p_2) \tag{3}$$

$$E_{s} = (1 - \mu_{s}^{2}) E_{D} \tag{4}$$

$$\phi' = 28 + 14.6 \log^2 K_D \tag{5}$$

Concrete

Concrete for the pile specimens and simulated rock blocks was delivered to the UCI experimental facility from a local plant in Orange County. The concrete aggregate consisted of pea gravel with a maximum size of 1 cm [3/8 in]. Slump values measured at the time of placement were 7.6 cm [3 in] for the rock-block concrete and 9.5 cm [3.75 in] for the pile concrete. Concrete cylinders with dimensions of 15 cm [6 in] in diameter by 30.5 cm [12 in] in height were taken on site per ASTM C39. The rock-block concrete mix had a 28-day design compressive strength of 34.5 MPa [5 ksi], and an average cylinder break strength of 48.3 MPa [7 ksi] on the day of testing. Pile Specimens 1, 2, and 3 had a 28-day design compressive strength of 27.58 N/mm² [4 ksi], and cylinder break

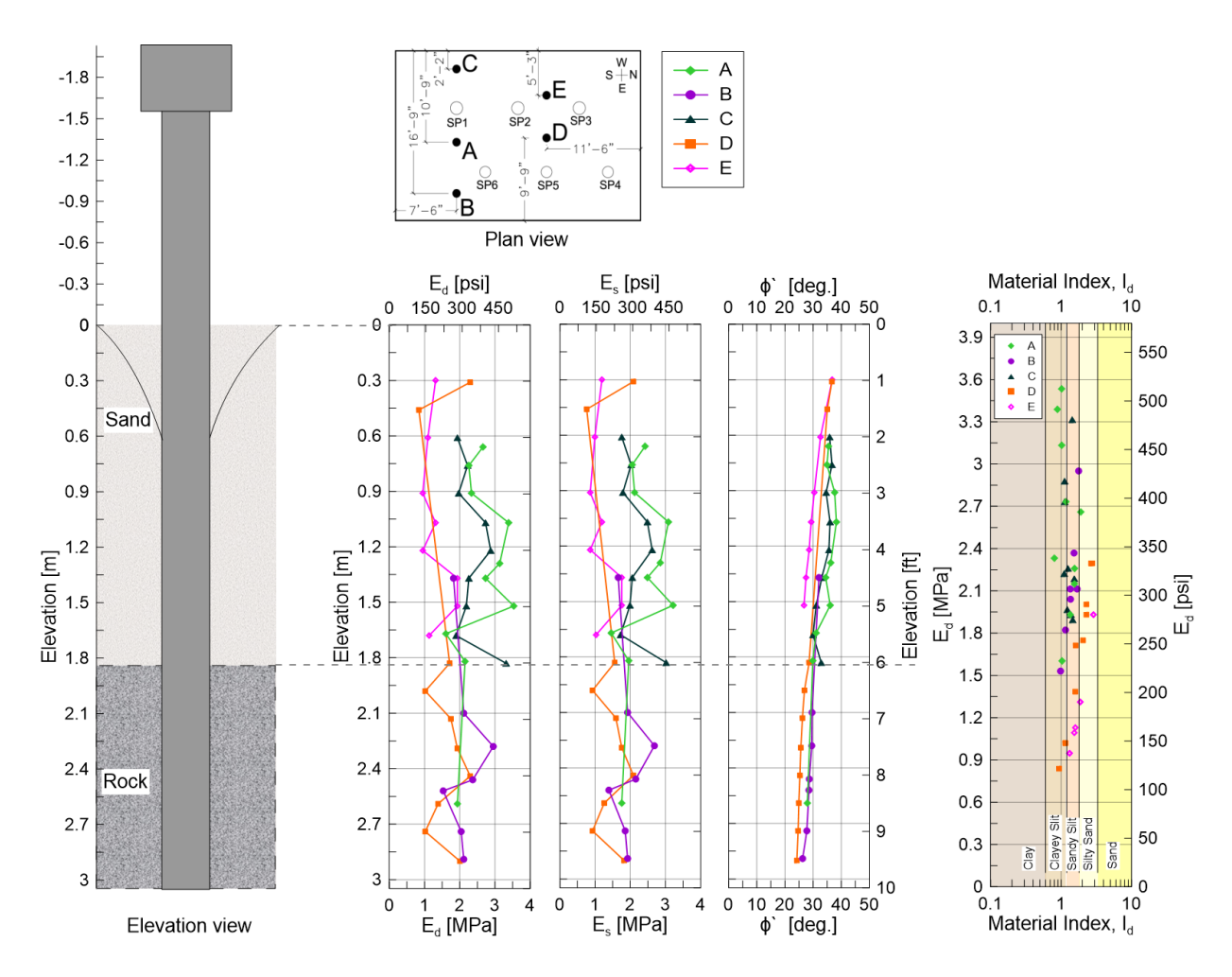


Figure 5. DMT test results at boreholes A, B, C, D, and E inside the soil pit

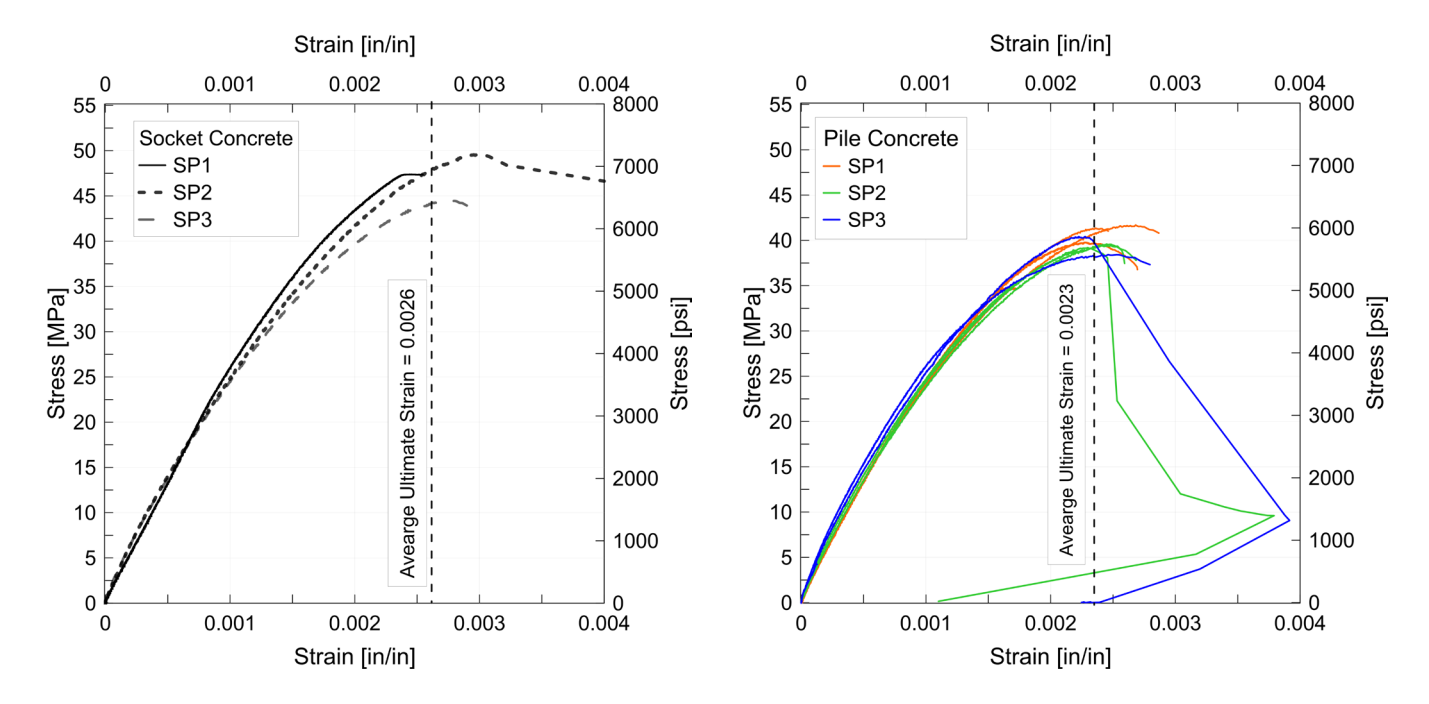


Figure 6. Compressive stress-strain relationship of rock-block concrete at the day of testing

Figure 7. Compressive stress-strain relationship of pile concrete at the day of testing

strengths of 40.7, 39.3, and 39.3 MPa [5.9, 5.7, and 5.7 ksi] on the day of testing, respectively. A summary of the average cylinder test results is shown in Figures 6 and 7. Young's modulus values measured from the concrete cylinders was $\rm E_{conc,pile} = 26.6~GPa~[3856~ksi]$ and $\rm E_{conc,rock} = 25.5~GPa~[3695~ksi]$. The ratio of rock to soil stiffness ($\rm E_{rock}/\rm E_{soil}$) is about 15,000.

Specimen Construction

Figure 8 shows photographs during specimen construction. The overall construction sequence consisted of first constructing the piles, then casting the simulated rock blocks around them; this is of course the opposite of normal construction procedures in which a drilled shaft is cast in a drilled hole, but was utilized here for convenience and to allow for care-



Figure 8. (a) Pile rebar cages, (b) Instrumented specimens prior to concrete pouring, (c) Concrete piles placed in rock-socket form-work, (d) Specimens with rock-sockets anchored into the floor (e) Pile cap prior to cap concrete pouring, (f) Geofoam blocks in place, (g) Sand pluviation, (h) Ramset setup for CPT/DMT testing, (i) Completed test setup for SP 1

ful specimen construction without damaging the extensive instrumentation network. After instrumenting all rebar cages outside the soil pit, the cages were placed inside Sonotubes and aligned along the wall of the soil pit (Figure 8b). Concrete was poured and manually vibrated to avoid sensor damage. The "pile caps" were constructed after the piles had cured for approximately one week. Along the socket lengths of the piles (1.22 m [4 ft]), the pile surfaces were roughened with a pneumatic needle scaler to improve adherence with the rock-block concrete and to better simulate the rough interface typical of a drilled rock socket. The piles were then placed and secured inside the rock-block formwork (Figure 8c) and the block concrete was poured as shown in Figure 8d. The hardened rock blocks were connected to the strong floor via high-strength steel anchors. The space between the rock sockets, which is unaffected by the lateral pile displacement since the rock blocks are anchored to the floor, was filled with geofoam (Figure 8f). The soil was placed in the pit by dry pluviation and leveled upon reaching the design height. Pre- and post-lateral load test in-situ investigations were performed to further characterize the fill material as explained in the previous section.

Pile Testing without Fill Soil

To validate the numerical input parameters and to better calibrate post-test numerical models, small amplitude lateral load testing without fill soil was conducted on specimen SP1. Figure 9 shows the test setup of the "nosoil" test. Prior to testing, the specimen's analytical moment-curvature $(M-\phi)$ relationships was blind-predicted using a variety of software tools, including Response2000 (Bentz, 2000), OpenSees (McKenna et al., 2000), and LPILE. The analytical M- ϕ relationships were estimated using the specified design material strengths, i.e., not the measured or overstrength values. The compressive strength was taken as 33.7 MPa [4.9 ksi], the concrete strain at maximum strength, ϵ_{c} was taken as 0.003, and the confined concrete compressive strength, f'cc was estimated as 44.13 MPa [6.4 ksi] following Mander et al.'s (1988) constitutive model. The reinforcement ultimate stress, yield strength, and yield strain were taken as 517 MPa [75 ksi], 413 MPa [60 ksi], and 0.002, respectively. Only one prediction was performed after concrete compressive testing was completed, which is labeled "post-test OpenSees" in Figure 10. This prediction uses a refined estimate of concrete strain at maximum strength using 0.002 instead of 0.003. Figure 10 shows a comparison of analytically and experimentally derived moment-curvature data. Lateral displacements were applied through the hydraulic actuator attached to the pile cap up to approximately 50% of the analytically predicted cracking displacement of the pile [0.13 cm, 0.05 in]. The corresponding applied lateral load was up to 3.6 kN [0.8 kips].

Load Application (Testing with Soil Fill)

The lateral loading protocol was developed based on the predictive analyses and followed the general guidelines of

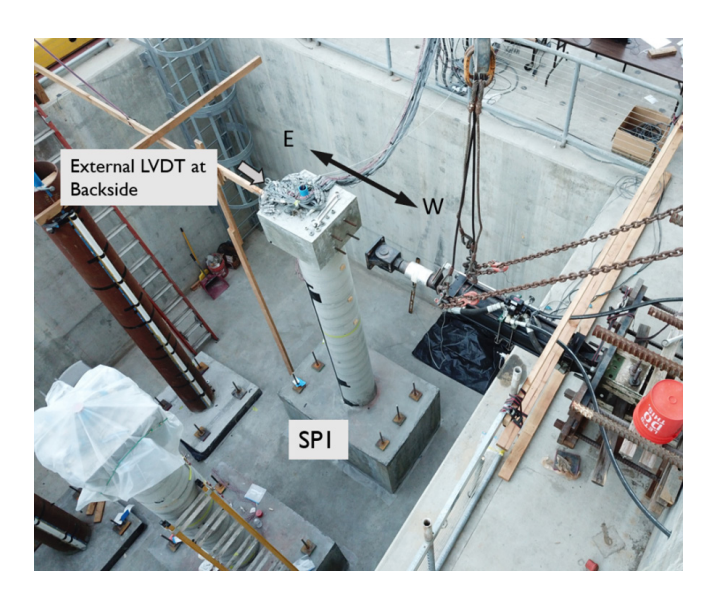


Figure 9. Specimen one lateral load test without backfill soil

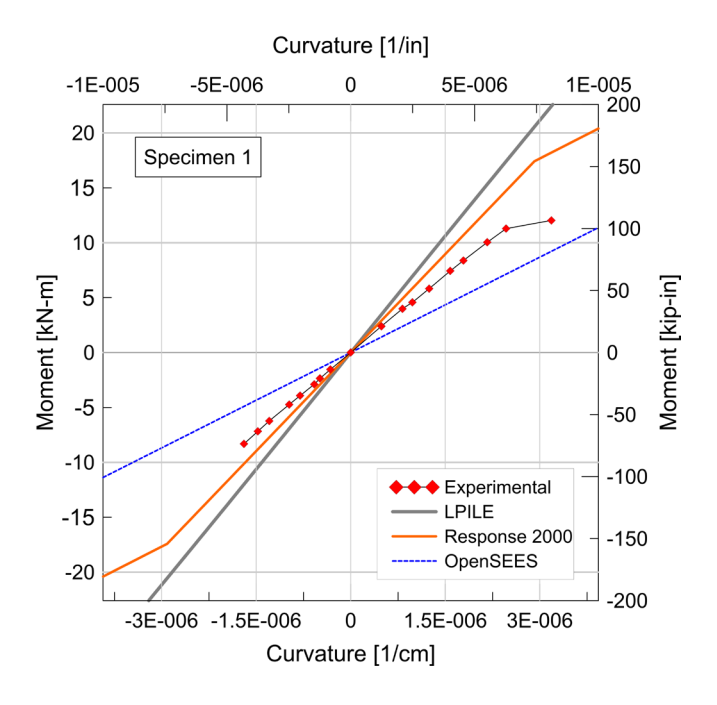


Figure 10. Comparison of analytically and experimentally derived moment-curvature data of SP 1 in the linear deformation range

the ASCE 41-17 (2017) recommendations in which applied lateral displacement levels are selected as fractions or multipliers of the anticipated yield displacement. This approach is most commonly used for the seismic evaluation of structures and simulated the earthquake loading through quasi-static fully reversed cycles with progressively increasing displacement amplitudes. Loading was applied at the pile head using three cycles per displacement level up to ultimate capacity. Hereafter, two cycles per displacement level were performed until substantial degradation of the lateral load-displacement relationship was noticeable as shown in Figure 12. Loading was applied under displacement control at the center of the

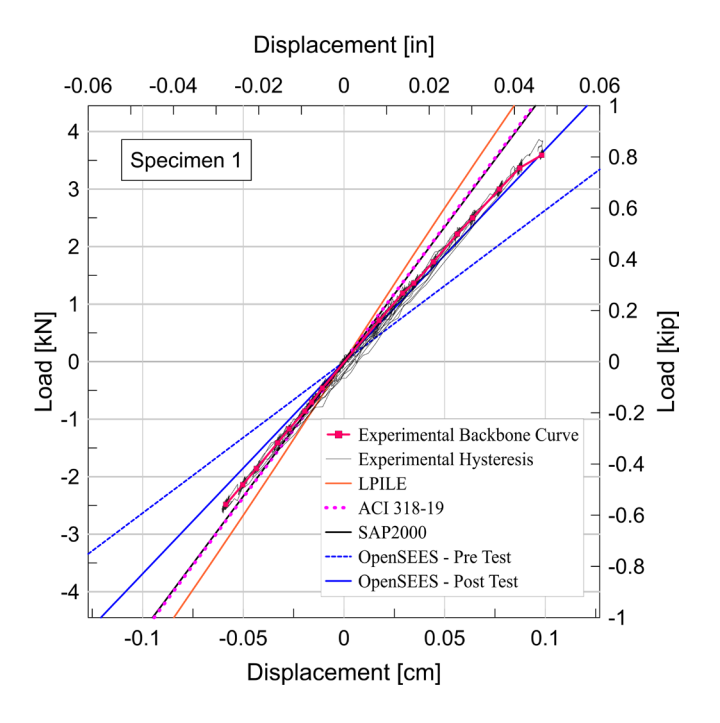


Figure 11. Comparison of analytically and experimentally derived load-displacement data of specimen one without backfill soil

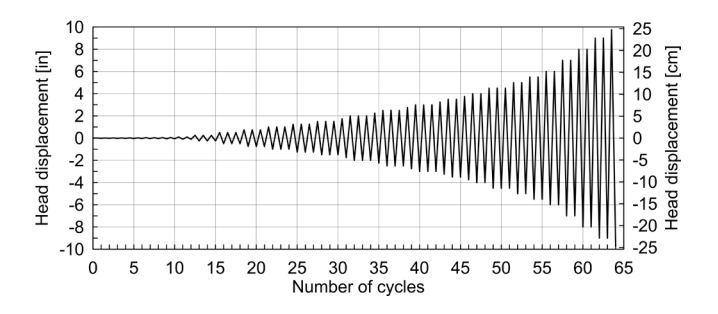


Figure 12. Pile head displacement history and loading cycles for SP1

pile cap using a 76.2-cm [30-in] stroke, 667-kN [150-kip] capacity hydraulic actuator (see Figures 8 and 9). The strong wall of the UCI laboratory served as a reaction wall to the loading setup. The actuator was controlled by an MTS 407 dual-channel controller and data were recorded using a National Instrument data acquisition system. A total of 115 channels were utilized for each test. An externally installed LVDT, mounted between an independent reference frame and the backside of the pile cap was used to control the experiment and record the pile head displacement.

Test Results

Post-Test Failure Observations

A spray-painted grid with dimensions of 15 x 15 cm [6 x 6 in] was applied to the sand surface around the pile specimen to monitor the extents of soil cracking, heaving, and caving. An example of the circumferential crack expansion and the formation of "crater-type" holes around the piles for lateral displacements larger than 10 cm [4 in] is depicted

in the photographs of Figure 13. Following test completion, each pile was manually excavated (in push direction) to identify cracking patterns and detect the presence and approximate location of plastic hinge(s) (Figure 13). Typical structural failure modes in a reinforced concrete shaft are classified into two dominant types, flexural failure or shear failure. Cracks associated with flexural failures start at the tension side of the specimen section and extend to the compression side. These cracks are mostly horizontal and are concentrated at the location(s) of maximum moment. Shear failure occurs when imposed shear stresses are higher than the section shear strength. In the case of shear failure of a rock-socketed drilled shaft, it would be expected that shear cracks would be concentrated at or slightly below the soil-rock interface. Shear cracks are conventionally understood to form at an angle, bending down towards the compression side of the cross section. For all three of the test specimens, the most substantial structural cracking was concentrated within 61 cm [24 in] above the rock socket but also extended to higher elevations at increasingly larger spacing. Almost all cracks formed perpendicular to the pile axis indicating a flexural mechanism; very few diagonal cracks that would be indicative of shear failure were recorded. No spalling was observed along the shaft circumference. In addition, there were no signs of cracking or damage along the socket surface or within the rock socket itself.

Load-Displacement Relationships

Figure 14 shows the experimental load-displacement behavior of all specimens with their respective backbone curves. Specimen 1 reached an ultimate load of approximately 72 kN [16.2 kips] at a pile head displacement of 17.8 cm [7.0 in] in the push direction, and approximately 72 kN [16.2 kips] at a pile head displacement of 20.0 cm [7.8 in] in the pull direction. Similarly, Specimen 2 reached ultimate resistance at 71 kN [16 kips] and 17.8 cm [7.0 in] in the push direction, and approximately 79 kN [17.8 kips] at a pile head displacement of 17.8 cm [7.0 in] in the pull direction. Specimen 3 reached an ultimate resistance of 77 kN [17.3 kips] at 20.0 cm [7.8 in] of lateral displacement in the pull direction and exhibited similar behavior in the push direction.

All specimens behaved essentially identically up to "concrete cracking", *i.e.*, up to a displacement level of 0.64 cm [0.25 in] and a corresponding load of 13.34 kN [3 kips] (about 20% of the ultimate load). The yield displacement was approximately 6.35 cm [2.5 in] at a corresponding load of 8 kips (about 50% of the ultimate load) after which the piles accumulated substantial permanent deformations for repeated loading cycles. Figure 14 includes a comparison between the experimental and predicted load-displacement curves as well as the applied pile-head load loads corresponding to predicted failure in flexure (SP1) and shear (SP2 and SP3). The experimental data show that the predicted failure loads have been exceeded by 23%, 53%, and over 100% for SP1, SP2, and SP3, respectively.

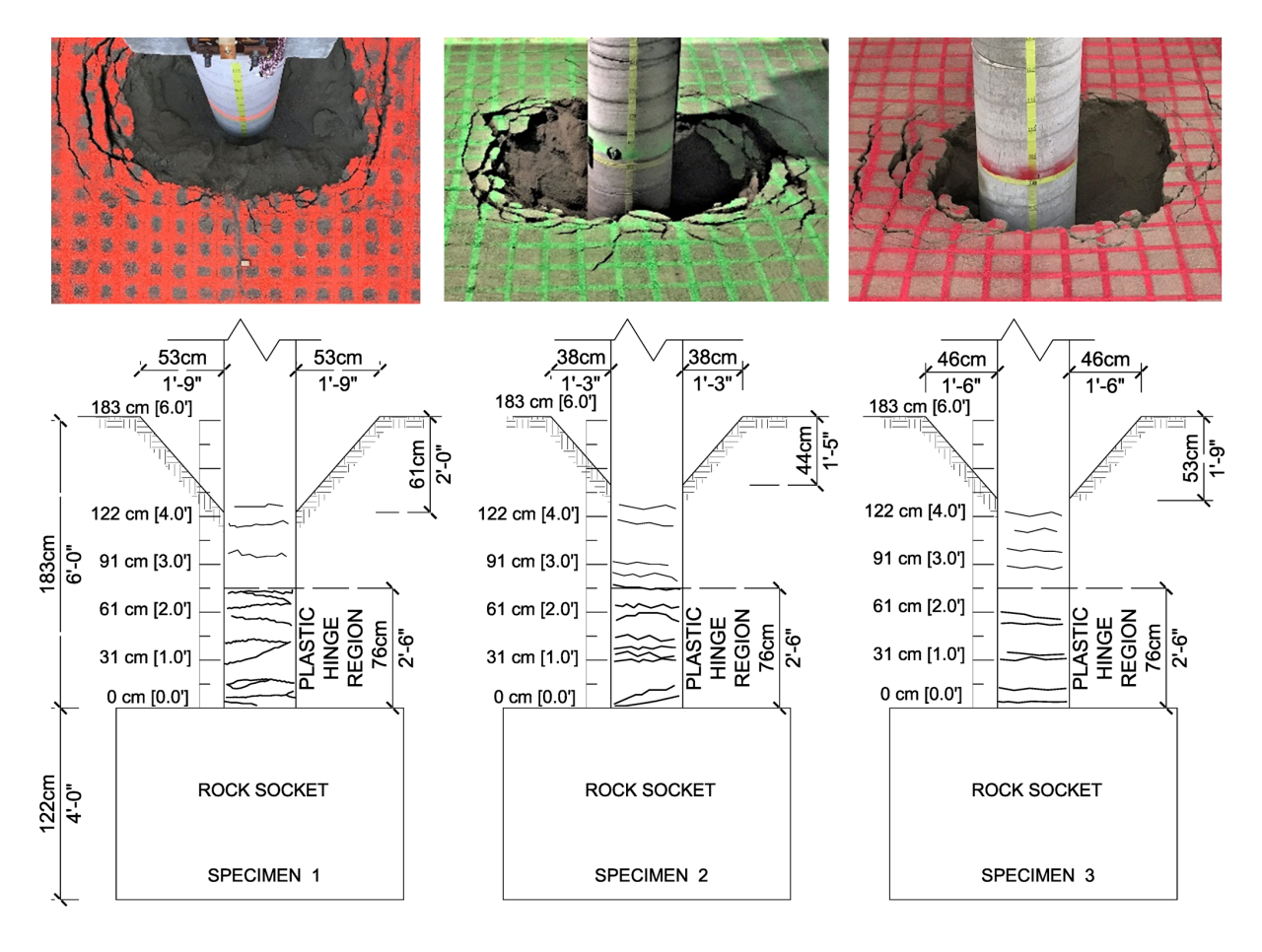


Figure 13. Major cracks along the pile depth and around the surface soil at test completion

The observed damage patterns and nearly identical load versus deformation behavior for the three specimens suggest that all specimens exhibited a flexural failure mechanism. Specifically, the predicted shear failure due to potential shear amplification near the rock-socket interface would have caused a much earlier failure of SP 2 and SP3 at applied pile head loads of approximately 52 kN [11 kips] and 35 kN [7.8 kips], respectively, which was not observed experimentally. Note that these failure predictions using the p-y method are based on as-built material properties as presented earlier in the manuscript, not specified nominal material properties. Instead, the pile specimens SP2 and SP3, which were insufficiently reinforced for the analytically predicted shear amplification, performed identically to the pile specimen SP1, which was sufficiently reinforced for the shear amplification. SP2 resisted a lateral ultimate load at failure of more than 1.3 times the predicted ultimate capacity based on shear failure and SP3 resisted a lateral ultimate load at failure of more than 2 times the predicted ultimate capacity based on shear failure.

Figure 15 shows the lateral deformation profiles recorded through the inclinometer. As expected, measurements indicate that insignificant deformation occurred within the rock socket. Small lateral pile deformations were noticeable beyond 15 cm [0.5 ft] above the rock

socket. Deformed shapes were similar for all specimens in both "pull and push" directions. Curvature profiles (not depicted for brevity) suggest the formation of a plastic hinge within 60 cm [2 ft] above the rock-socket which corresponds to 1.2 m [4 ft] below the ground surface (*i.e.*, about 3 pile diameters (3D); which also coincides with the plastic hinge location) and agrees well with crack patterns observed upon excavation and the maximum moment location shown in Figure 16.

Figure 16 shows a comparison of experimentally and analytically derived moment profiles for SP1. Experimental moment profiles were obtained using curvature data from strain gauge pairs (East/West, see Figure 4) at the same pile elevations. The curvature data were then multiplied with the nonlinear moment-curvature relationship to account for stiffness degradation upon concrete cracking. Figure 16 also shows the predicted moment profiles from the LPILE analysis for three selected lateral displacement levels. Predicted and back-calculated moment profiles agree relatively well, indicating the p-y method provides a reasonable estimate of flexural demands. Slight over-prediction of experimentally determined moments can be seen within the upper pile elevation for 5 cm [2 in] and in the lower section for 2.5 cm [1 in] lateral pile head displacements.

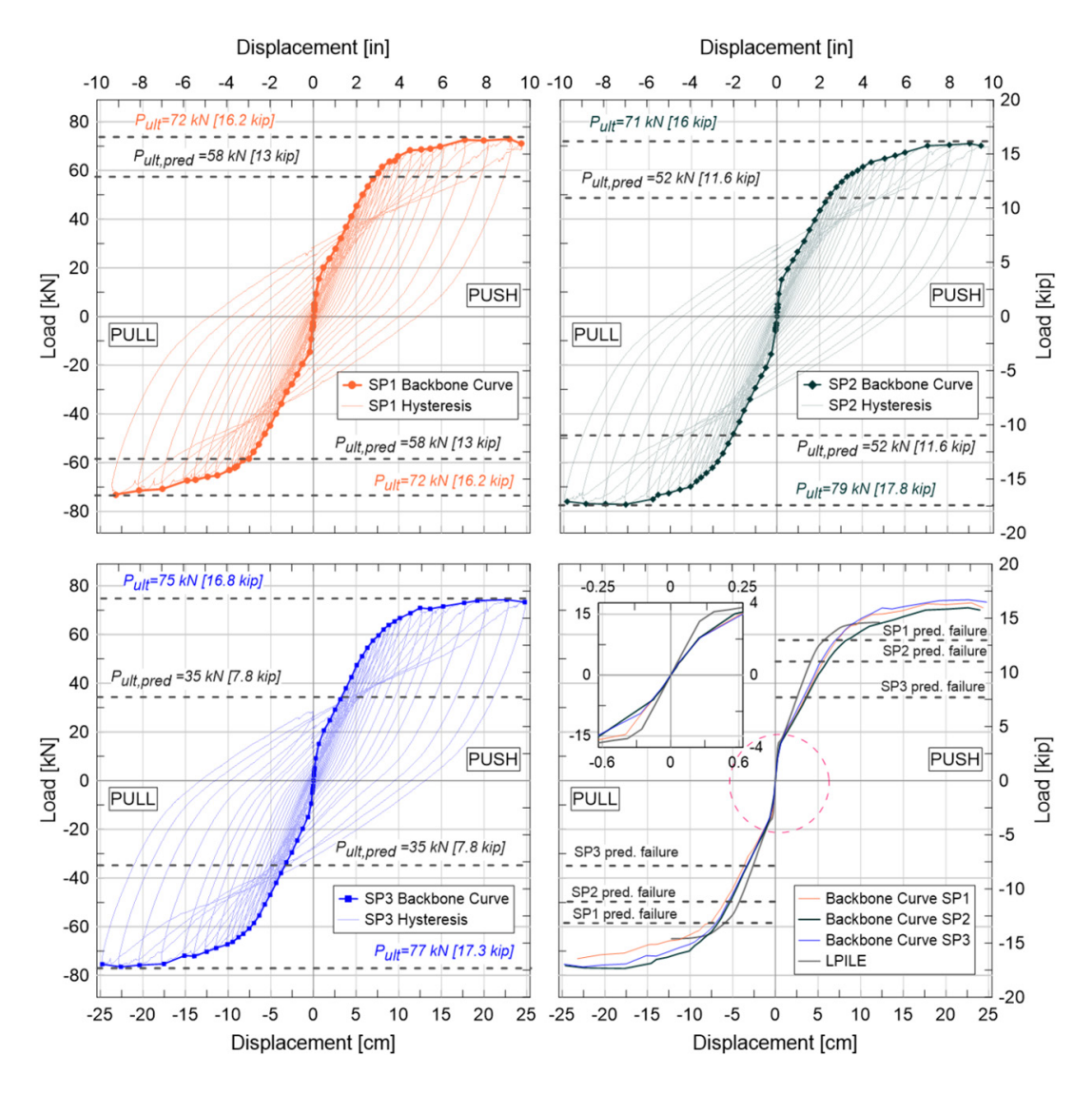


Figure 14. Experimental load-displacement relationships with backbone curves

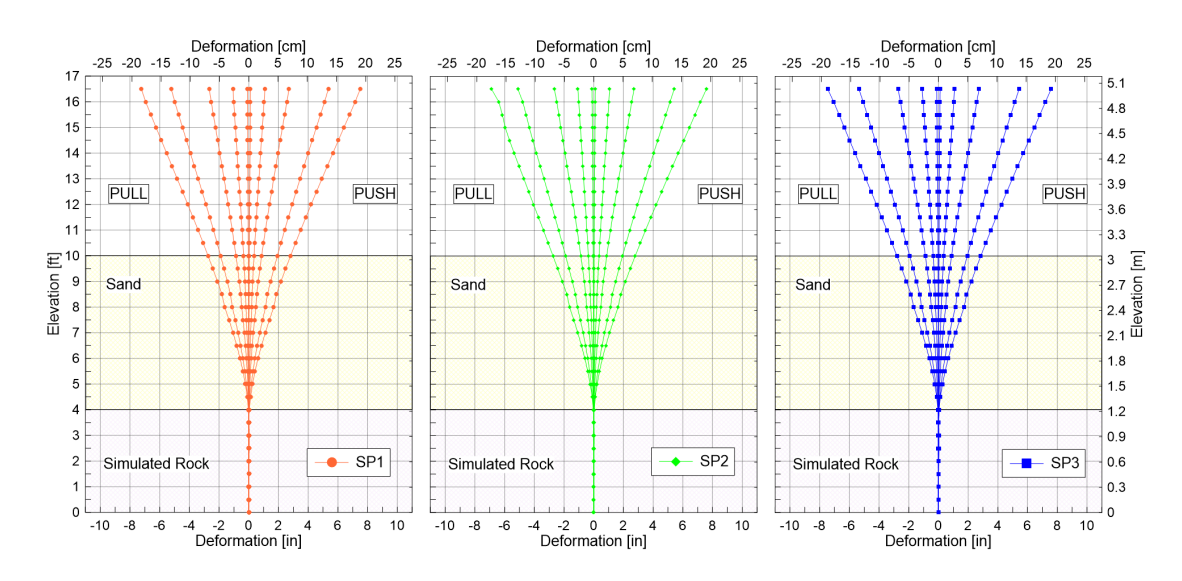


Figure 15. Deformed shape of Specimen 1 (left), Specimen 2 (middle) and Specimen 3 (right) at each applied displacement level (inclinometer readings)

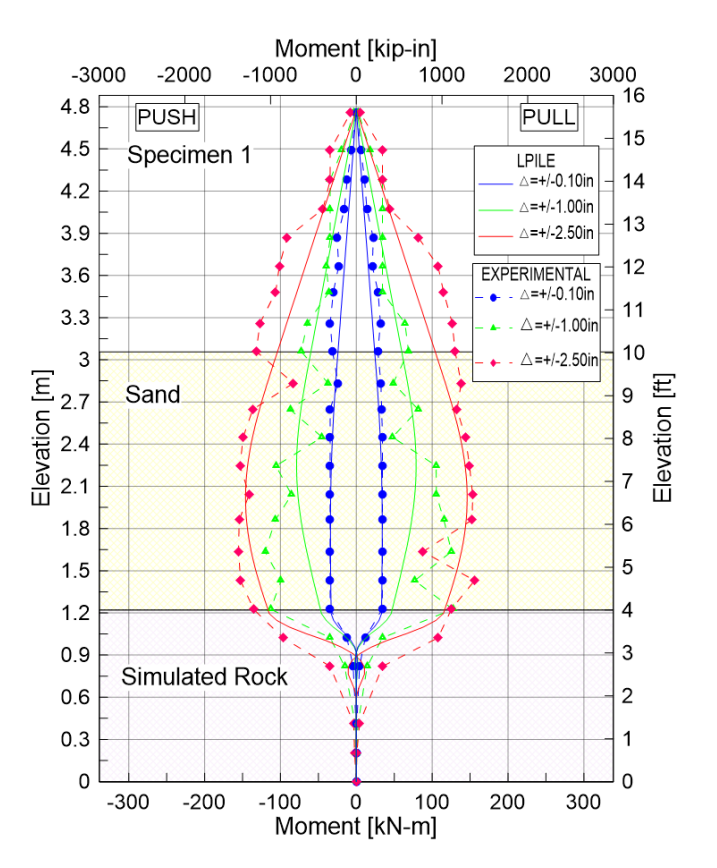


Figure 16. Comparison of analytically and experimentally derived moment-profile of specimen one

Summary and Conclusive Comments

Three pile specimens with different transverse shear reinforcement ratios were examined under identical test conditions and subjected to reverse cyclic lateral loading. The specimens were installed in a two-layer stratigraphy with a strong stiffness contrast consisting of loose sand underlain by rock, experimentally simulated by high-strength concrete. Specimens were loaded to complete structural failure and examined after test completion. No damage (i.e., cracking) and no lateral pile deformations were observed inside the rock socket. Predominantly flexural cracking occurred along the piles within 60 cm [2 ft] above the rock socket. This elevation corresponds to a depth of three pile diameters below ground surface, which is a typical location of plastic hinges of flexible piles. The differently reinforced pile specimens would be expected to fail in different failure modes according to their transverse reinforcement ratios and the predicted shear amplification using the p-v method. The experimental specimen behavior showed that the analytically predicted shear dominated failure did not occur. These preliminary observations could be of future benefit to the construction industry as bulky transverse reinforcement could be minimized and potential issues such as restrictions of concrete flow resulting in defective concrete due to closely spaced transverse reinforcement could be reduced. This study is limited to one configuration (one rock layer underlying one soil layer) and one shaft geometry with varying shear reinforcement ratios.

However, the extensive physical measurements collected from the variety of reliable sensor instrumentation allow for advanced parametric studies using a validated numerical model established on the test results presented herein. Numerical parametric studies are currently underway to develop response profiles beyond the configuration tested in this experimental investigation and to derive generalized design recommendation for a broad range of pile-soil-rock configurations and rock-soil stiffness contrasts. Additional structural limitations such as the lack of axial pile loading and the investigation of its effect on the structural behavior of the shaft has limited impact on the result of this experiment and can be accounted for numerically. Since the soil materials was placed in very loose densities, its contribution to the overall lateral pile-soil resistance is limited. A strict structural model of the horizontally loaded pile (without soil) provides very close response behavior to that observed in the experimental studies conducted by the authors. This is expected from a structural point of view. However, in common geotechnical design, soil is not omitted in the foundation model and leads to analytical response predictions as addressed in this study. The experimental observations highlight the importance of numerical assumptions and their consequences on construction performance.

Acknowledgment

The experimental work was funded through DFI's Committee project fund, as well as through Prof. Lemnitzer's NSF funding (CMMI 1752303), along with generous industry support from our colleagues at DFI and ADSC. We would like to gratefully acknowledge the members of the DFI Drilled Shaft Committee, many of whom provided continuous feedback and guidance during the design and construction process [specifically Committee Chair Paul Axtell (Dan Brown and Associates), Peter Faust (Malcolm Drilling), Dr. Eric Loehr (Univ. of Missouri), and Dr. Armin Stuedlein (Oregon State University)]. The OpenSees blind test predictions for the "no-soil test" were conducted at the University of Washington, Seattle, and we sincerely thanks Prof. Pedro Arduino and Dr. Long Chen for their collaboration. We are furthermore extremely grateful for the material and equipment donations as well as the engineering support by: PJ Rebar (Nathan King), Atlas Geofoam (Chris Franks), Williams Form Engineering (Pete Speier and Jeff Ohlsen), Foundation Technologies, Inc. (Nick Milligan) and Gregg Drilling and Testing (Brian Savela and Kelly Cabal). Without the support of these colleagues, this research program would not have been possible in the scope described.

References

American Association of State Highway and Transportation Officials, AASHTO (2017) AASHTO LRFD 8th Bridge Design Specifications. Washington, D.C.

American Concrete Institute. (2019). Building Code Requirements for Structural Concrete (*ACI 318-19*) and Commentary (ACI 318R-19)

- American Society of Civil Engineers (ASCE). (2017). "Seismic evaluation and retrofit of existing buildings", ASCE/SEI 41-17, Reston, VA.
- Arduino, P., Chen, L., and McGann, C. (2018). "Estimation of Shear Demands on Rock Socketed Drilled Shafts subjected to Lateral Loading", PEER Report, retrieved from https://peer.berkeley.edu/sites/default/files/2018_06_arduino_final.pdf
- Ashour, M., Norris, G., Bowman, S. Beeston, H. Pilling, P. and Shamsabadi, A. (2001). "Modeling pile lateral response in weathered rock", *Proceedings, 36th Annual Symposium on Engineering Geology and Geotechnical Engineering*, Eds Luke, Jacobson & Werle, University of Nevada, Las Vegas, March 28-30, 2001.
- ASTM C31 / C31M-18. (2018). "Standard Practice for Making and Curing Concrete Test Specimens in the Field", ASTM International, West Conshohocken, PA, www.astm.org
- ASTM D1557-12e1. (2012) "Standard Test Methods for Laboratory Compaction Characteristics of Soil Using Modified Effort (56,000 ft-lbf/ft3 (2,700 kN-m/m3))". ASTM International, West Conshohocken, PA, www.astm.org
- ASTM D3080 / D3080M-11. (2011). "Standard Test Method for Direct Shear Test of Soils Under Consolidated Drained Conditions". ASTM International, West Conshohocken, PA, www.astm.org.
- ASTM D6635-15. (2015). "Standard Test Method for Performing the Flat Plate Dilatometer". ASTM International, West Conshohocken, PA, www.astm.org.
- ASTM D5778-12. (2012). "Standard Test Method for Electronic Friction Cone and Piezocone Penetration Testing of Soils". ASTM International, West Conshohocken, PA, www.astm.org.
- Bentz, E.C. (2000). "Sectional Analysis of Reinforced Concrete Members," PhD Thesis, Department of Civil Engineering, University of Toronto, 310 pp
- Brown, D. A., Turner, J. P., Castelli, R. J., & Americas, P. B. (2010). Drilled shafts: Construction procedures and LRFD design methods (No. FHWA-NHI-10-016). United States. Federal Highway Administration.
- Brown, D., & Shie, C.-F. (1990). Three Dimensional Finite Element Model of Laterally Loaded Piles. *Computers & Geotechnics* 10, 59-79
- Caltrans, F. (2015). Bridge design practice, 4th edition. California Department of Transportation, Sacramento, CA.
- Carter, J.P. and Kulhawy, F.H. (1992). "Analysis of laterally loaded shafts in rock". *ASCE Journal of Geotechnical Engineering*, Vol. 118, No. 6, pp.270ff.
- Dykeman, P. and Valsangkar, A.J. (1996). "Model studies of socketed caissons in soft rock". *Canadian Geotechnical Journal* 33: 747-759

- Ensoft, Inc (2018) LPILE User's Manual. A Program to Analyze Deep Foundations Under Lateral Loading. Austin, Texas.
- Frantzen, J. and Stratten, F.W. (1987). *P-y curve data for laterally loaded piles in shale and sandstone*. Report No. FHWA-KS-82-2
- Gabr, M., Borden, R., Cho, K., Clark, S., and Nixon, J. (2002). "P-y Curves for Laterally Loaded Drilled Shafts Embedded in Weathered Rock", Technical Report, North Carolina Department of Transportation, Raleigh, North Carolina
- Guo, F. and Lehane, B.M. (2016). "Lateral response of piles in weak calcareous sandstone". *Can. Geotech. Journal*, 53: 1424–1434 dx.doi.org/10.1139/cgj-2015-0600
- Khosravifar, A. and Zafir, Z. (2019). "Modified strong rock p-y curves for rock socketed pile shafts". Deep Foundations Journal, Vol 13 (1), DOI 10.1080/19375247.2019.1595994
- Kim, D., Choo, Y.W., Kwank, K. (2015). "Comparison of lateral behavior of rock-scoketed large-diameter offshore momopiles in sand with different relative densities", *International Journal of Offshore and Polar Engineering*, Vol. 25(2), 156-160
- Leung, C.F. and Chow, Y.K. (2000). "Performance of laterally loaded socketed piles". Proceedings of the ISRM International Symposium, Melbourne, Australia, November 2000.
- Liang, R., Yang, K., and Nusairat, J. (2009). "P-y criterion for rock mass". Journal of Geotechnical and Geoenvironmental Engineering, 135(1):26-36, DOI: 10.1061/_ASCE 1090-0241 2009 135:1 26
- Mander, J. B., Priestley, M. J., & Park, R. (1988). "Theoretical stress-strain model for confined concrete." *ASCE Journal of Structural Engineering*, 114(8), 1804-1826.
- Marchetti S., (1997). "The flat dilatometer: Design applications." 3rd Geotechnical Engineering Conf., Keynote lecture, Cairo Univ., Cairo, Egypt, 421–448.
- McKenna, F., Fenves, G. L., Scott, M. H., and Jeremic, B. (2000). OpenSees Version 2.3.2 [Computer software]. Berkeley, Univ. of California. (http://opensees.berkeley.edu).
- O'Neill, M. W., & Murchison, J. M. (1983). "An evaluation of p-y relationships in sands." A Report to American Petroleum Institute, PRAC 82-41-1. University of Houston.
- Parsons, R.L., Willems, I., Pierson, M.C., Han, J. (2010). "Lateral capacity of rock sockets in limestone under cyclic and repeated loading" Report No. K-Tran: KU-09-06
- Reese, L. (1997). "Analysis of laterally loaded piles in weak rock". *ASCE Journal of Geotechnical and Geoenvironmental Engineering*, Vol. 123, No. 11

- Rojas-Gonzalez, L. F., Margules, P. A., and DiGioia, A. M. Jr. (1993). "Summaries of full-scale rock-socketed foundation tests." Rep.; RP1493-7, Electric Power Research Institute (EPRI), Palo Alto, Calif.
- Ramakrishna K., Karthigeyan, S., and Rajagopal, K. (2004). "Behavior of Rock Socketed Short
- Piles under Lateral Loads". Proceedings, Indian Geotechnical Conference 2004, Warangal, India, 17-19 December, retrieved from http://krc.cbri.res.in:8080/dspace/bitstream/ 123456789/492/1/GE13.pdf
- Yang, K., & Liang, R. (2006). "Numerical solution for laterally loaded piles in a two-layer soil profile". *Journal of Geotechnical and Geoenvironmental Engineering*, 132(11), 1436-1443.
- Yuan, S., Zhang, K., Liu, Z., & Li, J. (2014). Numerical tests on laterally loaded drilled shafts in socketed rock. *Advanced Materials Research Vols.* 919-921, 706-709.

DFI Journal Underwriters









